# Type Ia Supernovae

# 15

Kate Maguire

**Abstract**

Type Ia supernovae play an important role in many areas of astrophysics, as extragalactic distance indicators and the most mature probes of cosmic acceleration, as the main producers of iron in the Universe, as end points of stellar evolution, and as contributors to the chemical evolution of galaxies. While Type Ia supernovae have long been hypothesized to result from the thermonuclear explosions of carbon-oxygen white dwarfs, the stellar systems that produce these events and their explosion mechanisms are still very much under debate. The aim of this chapter is to describe the observational characteristics of Type Ia supernovae, ranging from their light curve and spectral properties to constraints from the galaxies within which they explode. Although they are a predominantly optical phenomenon, their observational signatures from gamma-ray to radio wavelength are discussed. An overview of the potential channels through which they could explode is also provided, along with the best current observational tests of the different scenarios. The use of Type Ia supernovae in modern cosmology, in the context of light curve-luminosity correlations, is also discussed.

## Contents

K. Maguire (✉)
Astrophysics Research Centre, School of Mathematics and Physics, Queen's University Belfast, Belfast, UK
e-mail: kate.maguire@qub.ac.uk

# 1      Introduction

Although there are many open questions that drive the field of Type Ia supernova (SN Ia) research, it is their importance as cosmological distance indicators for which they are best known. SNe Ia are currently the most mature probes of the expansion history of the Universe. In 2011, the Nobel Prize in Physics was awarded for the discovery of the accelerating Universe using SNe Ia (Perlmutter et al. 1999; Riess et al. 1998). This discovery suggests the presence of a mysterious quantity, "dark energy," that is acting against gravity to push the Universe apart. This has led to large samples of SNe Ia being observed and from which the diversity and properties of SNe Ia can be studied in great detail. In this chapter, a brief introduction to their explosion physics and power source is first described. The main observational characteristics of SNe Ia are discussed, including their light curve and spectral properties from soon after explosion to a few years later, the empirical correlations used to standardize their light curve for use as distance indicators, as well as their observed signatures from gamma-ray to radio wavelengths.

## 1.1      Explosion Overview

Although SNe Ia play a fundamental role as cosmological distance indicators, there remain many open questions about their formation mechanism. For a long time, it was theoretically hypothesized that the star that explodes to produce a SN Ia is a carbon-oxygen white dwarf (Woosley et al. 1986), but there was no direct observational evidence for this. However, observations of the early-time light curves of the very nearby and very well-studied SN Ia, SN 2011fe, demonstrated for the first time that the primary star was a degenerate compact star, most likely a white dwarf (Bloom et al. 2012).

The nature of the explosion mechanism that produces SNe Ia is still controversial, with the two main competing channels being the single- and double-degenerate scenarios. In the double-degenerate channel, the companion star to the carbon-oxygen white dwarf is another carbon-oxygen white dwarf. In the single-degenerate channel, the companion star is a main sequence, subgiant, or giant star. Almost

all explosion models involve the transfer of mass, either steadily or violently, onto the primary white dwarf, which in some manner triggers a runaway thermonuclear explosion that unbinds the white dwarf.

In the classical view of a "Chandrasekhar mass explosion," the carbon-oxygen white dwarf accretes matter from its companion until it approaches the Chandrasekhar mass. At $\sim 1.37\,M_\odot$, carbon burning is ignited, triggering a subsonic ("deflagration") flame that propagates through the ejecta. As fusion of carbon and oxygen proceeds, the temperature of the star starts to rise. Since the degeneracy pressure of the white dwarf is independent of temperature, it cannot regulate the fusion process, and a runaway thermonuclear reaction is triggered. The nature of this transformation from subsonic deflagration to supersonic detonation ("delayed detonation") is not well understood.

In the Chandrasekhar mass model, all SNe Ia explode at approximately the same mass, producing the same amount of nuclear energy ($\sim 10^{51}$ erg) when the star is unbound. No compact remnant is expected to remain. Since all SNe Ia produce similar amounts of energy, they should all have similar absolute luminosities and, therefore, could be used as "standard candles" to measure distances in the Universe. In reality, the physics is more complicated and SNe Ia are not perfect "standard candles" – empirical correlations must be applied to correct their luminosities and enable their use as precision distance indicators.

## 1.2    Power Source

The observed emission of a SN Ia is powered by the radioactive decay of Fe-group elements that are synthesized in the explosion (Colgate and McKee 1969). The explosion itself is not observed, with the energy source being purely nuclear ($\sim 10^{51}$ erg). A large fraction of the inner region of the white dwarf is completely burned to produce mainly radioactive $^{56}$Ni, while the outer layers burn to produce intermediate-mass elements such as Si, Ca, S, and Mg.

The SN luminosity is powered entirely by the radioactive decay of elements produced in the explosion. It is powered first by the decay of $^{56}$Ni to $^{56}$Co, with a half-life of 6.1 days. This $^{56}$Co then decays, with a half-life of 77.3 days, to produce stable $^{56}$Fe. On average, $\sim 0.3$–$0.8\,M_\odot$ of $^{56}$Fe is produced in an SN Ia explosion (measured from their bolometric light curves or late-time spectra), making them the main producers of Fe-group elements in the Universe. The typical bolometric luminosity of a SN Ia is of the order of $10^{43}$ erg s$^{-1}$, with the majority of the light ($\sim 85\,\%$) being emitted at optical wavelengths.

Prior to maximum light, most of the energetic products (gamma rays, positrons) produced by radioactive decay are trapped within the ejecta (due to its high density), where they are reprocessed by interactions into optical and near-infrared (NIR) photons. The peak of a SN Ia light curve is powered by the decay of $^{56}$Ni, and the peak luminosity is directly proportional to the mass of $^{56}$Ni produced in the explosion. This relation is known as "Arnett's rule" (Arnett 1982).

With time, as the ejecta expands and the density drops, the fraction of gamma rays that escape increases. Between 80 and 200 d after maximum light, the energy deposition due to positrons (which is less important at early times) begins to dominate over that of the gamma rays. While the gamma rays can travel a long way before being absorbed in the low-density ejecta, positrons deposit most of their energy locally – the exact amount is likely to depend on the configuration of any magnetic field present.

## 2 Observational Characteristics

Since most of the luminosity of SNe Ia is emitted at optical wavelengths, this is where the majority of observations have focused. Photometric data points are typically obtained in broadband optical filters. Historically, Bessel filters (*UBVRI*) were used for the first low-redshift SN Ia samples. However, higher-redshift SN surveys such as the SN Legacy Survey (SNLS) and the Sloan Digital Sky Survey (SDSS) used *griz* filters, and these have now become the standard filters for nearly all SN surveys, as well as for follow-up measurements.

The spectral features of SNe Ia are broad due to their high expansion velocities, and therefore, high-resolution observations are not generally required. Typically SNe Ia are classified and followed up spectroscopically with a low-resolution setting, $\lambda/\Delta\lambda$ of ~300–700. This range maximizes the signal to noise of the spectrum, while still providing sufficient information about the broad SN features.

### 2.1 Discovery and Detection of SNe Ia

In recent years, the number of SNe Ia discovered by dedicated transient surveys has increased exponentially. This is due to a combination of dedicated survey telescopes tuned to discover SNe, as well as the increased efficiency of nonprofessional astronomers in finding SNe. SN Ia surveys typically aim for a time between observations ("cadence") of 2 to 5 days, since SNe Ia do not vary significantly on timescales smaller than this. A non-exhaustive list of recent and ongoing optical imaging surveys for astronomical transients (including SNe Ia) includes the Carnegie Supernova Project, Dark Energy Survey, La Silla Quest Variability Survey, (intermediate) Palomar Transient Factory, Pan-STARRS, SDSS, SNLS, and SkyMapper. These surveys have typical lifetimes of 2–5 years and have found (or will find) on the order of 100–1000 SNe Ia each.

When a potential transient that passes certain quality cuts (human and software based) is discovered in optical imaging, it is scheduled to be observed spectroscopically. Classification spectra are generally obtained at optical wavelengths (sometimes in the NIR). SNe are typically classified based on the properties of their optical spectra around maximum brightness (Filippenko 1997).
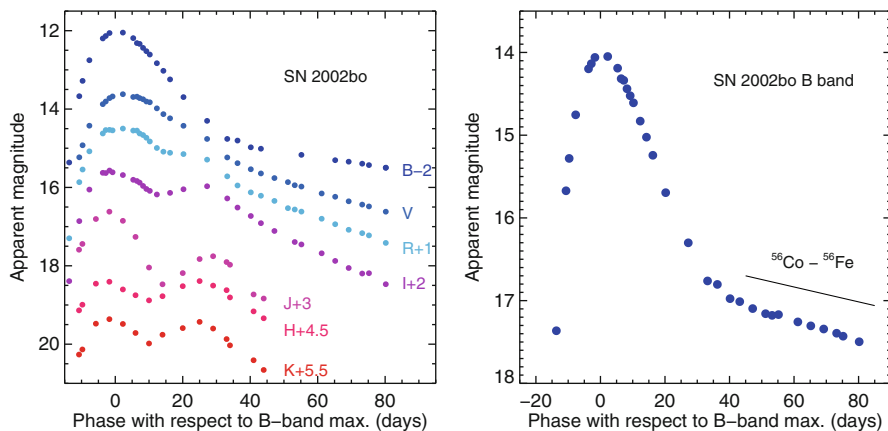
**Fig. 1** *Left panel: BVRIJHK* band light curves of a normal SN Ia, SN 2002bo. Optical data is taken from Ganeshalingam et al. (2010) and near-infrared data from Krisciunas et al. (2004). *Right panel:* The *B*-band light curve of SN 2002bo is shown. A risetime in the range 15–20 d is seen, followed by a steep decline after maximum for ∼30 d, before the light curve settles onto the radioactive decay tail of $^{56}$Co to $^{56}$Fe (see Sect. 1.2 for more details)

## 2.2 Light Curves

The optical light curves of most SNe Ia are very homogenous, following a similar evolution with time. They typically rise to maximum luminosity in the *B*-band in ∼20 days, with a slow decline after maximum light. After ∼50 days, the light curves start to follow an exponential decay, declining at a rate of about one magnitude per month. The optical through NIR (*BVRIJHK*) light curves for a normal SN Ia, 2002bo, are shown in Fig. 1 (left panel). In the right panel of Fig. 1, the *B*-band light curve is plotted, showing a rise to maximum light followed by a steep decline before joining the radioactive decay tail. The use of SNe Ia as cosmological distance indicators relies on that fact that their absolute magnitudes can be standardized using empirical corrections based on their light curve evolution.

### 2.2.1 Very Early-Time Light Curves

It was originally hypothesized that the luminosity of the early light curves of SNe Ia should scale to the surface of an expanding fireball, producing a luminosity that increases as $t^2$, where t is the time since explosion. However, Piro and Nakar (2014) showed that the assumptions necessary to produce this relation are not robust, and it is more likely that the power index varies from object to object, depending on the distribution of $^{56}$Ni in the ejecta and on the shock velocity. This is in agreement with observations where a range of power indices (1.5–3.7) are found for the early-time light curves of SNe Ia (Firth et al. 2015).

When an SN Ia explodes and the ejecta expands, a thermal diffusion wave travels back through the ejecta. At any given time, material above this wave is heated

mainly by the gamma rays from the radioactive decay of $^{56}$Ni and produces the observed luminosity of the SN. Any material below this wave only contributes to the observed luminosity if photons can diffuse out. If the $^{56}$Ni is located deep within the ejecta, then there may be a "dark phase" between the time of actual explosion and the emergence of the first photons. A dark phase of ∼1 day was inferred for SN 2011fe (Mazzali et al. 2014).

### 2.2.2 Light Curve Width-Luminosity Relation

After the first hours to days, the light curves of "normal" SNe Ia are very homogenous with little variation between objects. A key development in their use as distance indicators was the discovery of an empirical relation between SN Ia luminosity at maximum light and light curve width, which reduced the scatter in their absolute magnitudes (see Fig. 2). Before correction, normal SNe Ia span a reasonably wide range of luminosities, with absolute magnitudes in the range −18 to −19.5 mag. After corrections for light curve width (as well as color, see Sect. 2.2.3), the mean absolute SN Ia $B$-band magnitude is −19.05 ± 0.02 mag (Betoule et al. 2014).

More luminous SNe Ia have broader light curves, while fainter SNe Ia have narrower ones. This was first quantified by measuring the difference in the $B$-band magnitude of a SN Ia at maximum light and 15 d after maximum light, the so-called $\Delta m(B)_{15}$ (Philipp 1993). Since then updated measurements of this parameter (e.g., $\triangle$, $s$ and $x_1$) incorporating information from other bands, as well as the overall light



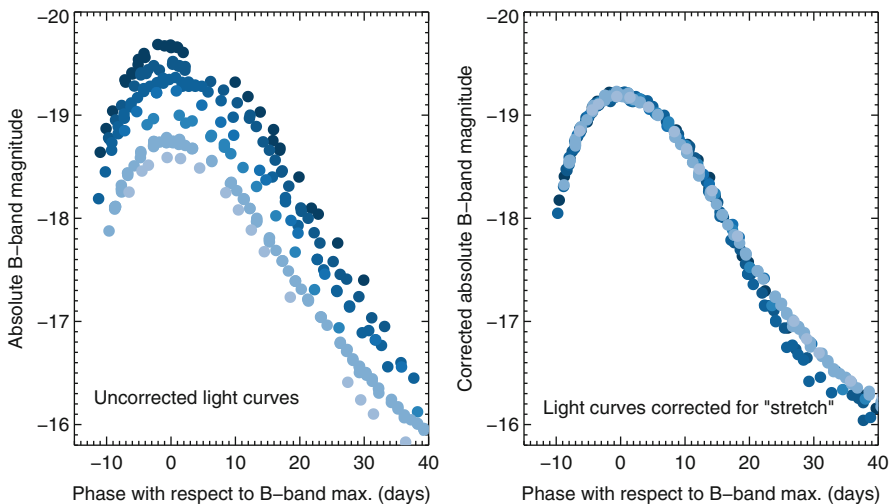**Fig. 2** *Left panel:* $B$-band light curves of a sample of SNe Ia with data taken from Hicken et al. (2009) and Stritzinger et al. (2011). The trend between light curve width and increasing absolute $B$-band magnitude is clearly seen. *Right panel:* The light curves from the left panel have been corrected for the measured light curve width, "stretch." The scatter in the absolute magnitude at peak is reduced

curve shape, have been measured using different light curve fitters, MLCS (Jha et al. 2007; Riess et al. 1996), SALT2 (Guy et al. 2005), and SIFTO (Conley et al. 2008).

As discussed in Sect. 1.2, the peak luminosity of the light curve is directly proportional to the mass of $^{56}$Ni synthesized in the explosion. The broadness (width) of the light curve is mainly determined by the diffusion time (how long it takes for photons to escape the ejecta), which depends on both the amount of Fe-group material produced in the explosion and the temperature of the ejecta (Hoeflich et al. 1996; Kasen and Woosley 2007). SNe Ia that produce more Fe-group elements have higher opacities and longer diffusion times and, therefore, keep the light curve brighter for longer, resulting in a broader peak.

Temperature differences also affect the light curve width. As the temperature of the ejecta drops after maximum light, the ejecta recombines from doubly to singly ionized species, and Fe II/Co II absorption features become important, particularly in the *B*-band where they absorb strongly. Since less luminous SNe Ia have, on average, cooler temperatures, the transition to Fe II/Co II occurs earlier in these SNe Ia. This results in a faster redistribution of flux to longer wavelengths in less luminous SNe Ia and therefore a faster *B*-band decline after maximum.

### 2.2.3 Light Curve Color-Luminosity Relation

In addition to the observed width-luminosity relation, a correlation between the $B$-band luminosity and the $B - V$ color measured at maximum light was identified (Tripp 1998) brighter SNe, on average, have bluer colors. The size of this correlation is larger than the width-luminosity relation and is the dominant correction applied to decrease the dispersion of SN Ia light curves for cosmology. For some SNe Ia, the likely cause of the relation between their $B - V$ color at maximum and their luminosity is due to dust attenuation that makes their light curves both redder and fainter. However, studies of low-reddening SN Ia samples have found this is not the main driver of the correlation for most SNe – it is most likely due to something intrinsic to the SNe themselves that results in more luminous SNe Ia having, on average, bluer colors. There is no significant observed correlation between light curve width and color at maximum for normal SNe Ia.

## 2.3 Spectra

The maximum-light spectra of SNe Ia are identified by a lack of H and He features and characterized by blueshifted absorption features of neutral and singly ionized intermediate-mass elements. The expansion velocities decrease with time. Different features have different measured velocities, suggesting a layered structure of the elements. With time, the contribution from Fe-group elements increases. As the ejecta expands, the outer layers become optically thin, and we can see deeper into the core of the ejecta where the Fe-group elements were produced.

The ejecta is typically moving with velocities of a few thousand kilometers per second, resulting in broad emission and absorption features. The velocity of material is generally measured from the minimum of the absorption features of different

species, either by fitting the line profile or through spectral modeling. Material that is farther out in the ejecta is moving faster. Assuming the ejecta is in homologous expansion, the velocity multiplied by the time since explosion gives the radius at which the material is emitting. Therefore, the radius and velocity can be used interchangeably as the spatial coordinate.

### 2.3.1 Early-Time Spectra

Early-time spectra (at least 5 days before maximum light) are characterized by absorption features of intermediate-mass elements such as silicon, calcium, magnesium, sulfur, and oxygen, with velocities in the range of $\sim$10,000 to 25,000 km s$^{-1}$. The earliest spectrum of a SN Ia was obtained for the very nearby, SN 2011fe, at just 1.5 d after the estimated explosion date (Nugent et al. 2011). This spectrum showed the first detection of high-velocity O I features, which is expected to originate from unburnt progenitor star material. Features consistent with carbon absorption were also seen. The presence of unburnt carbon and oxygen provides evidence that the exploding star was a CO white dwarf. The feature of carbon that is commonly studied is the C II 6580 Å feature, which is located at the red edge of the Si II 6355 Å feature (Fig. 3). Greater than 30 % of SNe Ia show C features if observed before $-5$ d with respect to maximum light (Thomas et al. 2011).

High-velocity features of Ca II, and sometimes Si II, are also seen in most SNe Ia when observed before maximum light (Fig. 3). These features typically
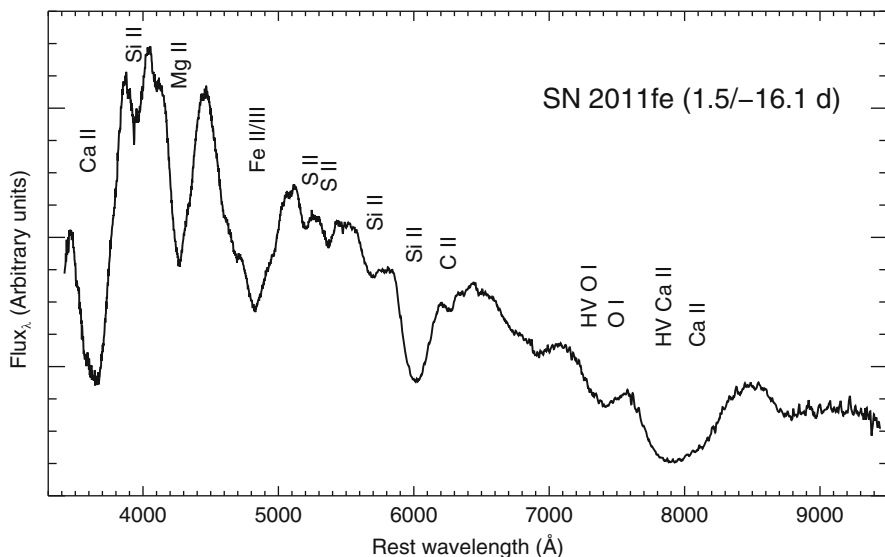


**Fig. 3** Optical spectrum of SN 2011fe from Nugent et al. (2011) at +1.5 days after explosion ($-16.1$ days with respect to maximum light). The main spectral features are labeled. High-velocity components of the O I and Ca II features are marked as "HV O I" and "HV Ca II," respectively. SN 2011fe was shown to require high-velocity components of C II, Mg II, Si II, and S II at this phase

are defined by being significantly above the photospheric component with typical velocities of $>15{,}000\,\mathrm{km\,s^{-1}}$. These features can sometimes be identified as distinct absorption features in their spectra. They are easiest to measure in the Ca NIR triplet feature (8498, 8542, 8662 Å), since the Ca II H&K feature (3933, 3969 Å) is contaminated by other features. However, the Ca NIR triplet feature can often only be disentangled by line-profile fitting. The origin of these high-velocity features is not well understood with possible explanations including circumstellar material around the SN, density, or abundance enhancements intrinsic to the SN ejecta (e.g., Gerardy et al. 2004; Mazzali et al. 2005).

### 2.3.2    Around Maximum-Light Spectra

By maximum light, the optical spectra of SNe Ia appear cooler (the continuum is less blue), but they are still dominated by intermediate-mass elements. There is a remarkable homogeneity in SN Ia spectra around maximum light. Some of the most prominent absorption features at these times are produced by Si: the Si II 6355 Å, Si II 5972 Å, and the Si II 4130 Å lines. Strong lines of Ca II are also seen in the spectra. However, this does not necessarily mean large quantities of Ca are present since only small amounts are needed to produce the strong Ca II features that are seen.

At maximum light, the SN ejecta is typically moving with velocities of 8000–$15{,}000\,\mathrm{km\,s^{-1}}$. High-velocity features of Ca II may still be visible, but their velocities are decreasing quickly with time. By about a week after maximum light, Fe lines start to become visible in the SN spectra, and within two weeks of maximum light, Fe absorption starts to dominate.

SN Ia spectral differences around maximum light arise mostly in the strengths and velocities of the strongest features present (Fig. 4). Variations in temperature and ionization state can be measured through the ratio of the Si II 5972 Å to the 6355 Å line strength, with a stronger Si II 5972 Å relative to the 6355 Å arising in cooler SNe Ia (Nugent et al. 1995). The presence of an O I feature at 7774 Å can be used to crudely distinguish SN Ia of different luminosities; it is most prominent in lower-luminosity SNe Ia and very weak in more luminous events.

### 2.3.3    Spectral-Luminosity Indicators

Various methods of estimating SN Ia luminosities by constraining the strengths and velocities of prominent spectral features have been proposed. One of the main aims of studying these spectral luminosity indicators is to improve upon purely photometric calibrators of the SN luminosities. Methods using different spectral properties have resulted in varying degrees of significance when correlated with SN brightness. The ratio of the Si II 5972 Å line to 6355 Å line strength at maximum light, as well as the strength of the Si II 4130 Å line, has been shown to correlate with the SN luminosity. However, as the size of SN samples increased, more and more SNe Ia were discovered that did not follow these previously identified correlations, suggestive of a greater diversity than previously expected. Given the increased time needed to obtain spectra compared to photometry, as well as the generally low
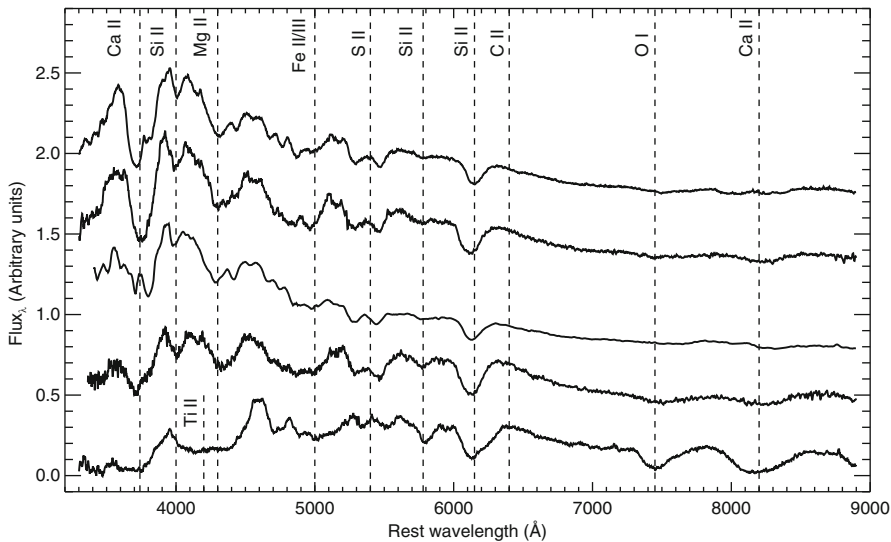
**Fig. 4** The diversity of features in a sample of maximum-light SN Ia spectra from Maguire et al. (2014) is shown. The dominant features contributing to the spectra are shown. The spectra are ordered from most luminous at the top to the least luminous at the bottom, with light curve stretch values in the range, $0.7 < s < 1.1$. The strength of the Si II 5972 Å relative to the 6355 Å is seen to increase down the spectral sequence toward cooler SNe Ia. In the least luminous SN Ia in the sample, the O I 7774 Å feature is strongest and Ti II absorption is identified at bluer wavelengths

levels of significance in the correlations, it appears unlikely they will provide much increased constraints over well-calibrated photometric measurements.

### 2.3.4 Late-Time Spectra

At epochs greater than $\sim$150 d, the outer layers of the ejecta have become transparent, and we can see deep into the inner ejecta layers. This is referred to as the "nebular phase." The SN luminosity at these epochs is powered by the radioactive decay of $^{56}$Co, producing gamma rays and positrons. Under nebular conditions, the energy deposition by gamma rays and positrons is balanced by cooling through line emission. The spectra of SNe Ia at late times are dominated by forbidden Fe-group emission lines.

Shifts of a few $1000 \, \text{km s}^{-1}$ (in some cases to the blue and in some to the red) in the central line position of the emission features with respect to the rest wavelength have been identified. This has been interpreted as due to an off-center ignition of the explosion (Maeda et al. 2010). Modeling of the spectra also allows constraints to be placed on the location of stable and unstable material, as well as the density structure of the ejecta. This can provide information about the explosion mechanism – in the case of SN 2011fe, modeling of its late-time spectra suggested a best match to a low-energy delayed detonation of a Chandrasekhar mass white dwarf (Mazzali et al. 2015, and Fig. 5).

**Fig. 5** Nebular optical through NIR spectrum from SN 2011fe at 250 days past max (*black line*) (Mazzali et al. 2015). The *blue line* is the best fit model with a high central density. The spectrum is dominated by forbidden lines, in particular [Fe II] and [Fe III] (Reprinted with permission from Mazzali et al. 2015 and Oxford University Press)

An infrared catastrophe, where the cooling of the ejecta below a certain critical temperature causes a shift in emission from optical and NIR transitions to mid- and far-infrared fine-structure transitions, was first predicted by Axelrod (1980). This shift in emission to longer wavelengths, however, was not observed in the few SNe Ia with the necessary late-time ($>500$ d) observations (e.g., Sollerman et al. 2004). More detailed spectral modeling has shown that while this shift to longer wavelengths does occur, it is balanced by nonlocal radiative transfer that converts most of the ultraviolet (UV) flux into optical and NIR emission (Fransson and Jerkstrand 2015).

## 2.4    Infrared Properties

The NIR (*IYJHK* filters) light curves of normal SNe Ia are characterized by a secondary peak 20–30 d after maximum light (see Fig. 1). At the time of this secondary maximum, the contribution from NIR wavelengths to the SN luminosity is at a maximum, accounting for $\sim$20 % of the optical luminosity (Wang et al. 2009). In normal SNe Ia, the primary peak in the NIR bands occurs before those

of the optical by $\sim$5 d. SN Ia NIR light curves around maximum are found to be remarkably homogenous, with a small intrinsic scatter ($\sim$0.09 mag scatter in the $H$-band). This small scatter in their absolute magnitudes is caused by a combination of the much lower attenuation by dust at NIR compared to optical wavelengths, as well as a smaller dispersion in the intrinsic properties of SNe Ia at these wavelengths.

While the diversity in the optical luminosity at maximum light is driven by differences in the $^{56}$Ni mass produced in the explosion, the NIR light curves at a similar epoch appear relatively insensitive to the $^{56}$Ni mass. Instead their homogeneity can be explained by the fact that SNe Ia with less $^{56}$Ni mass are not only fainter but also cooler, meaning they radiate a larger proportion of their energy at NIR wavelengths compared to brighter SNe Ia. A large dispersion is seen in both the timing and luminosity of the secondary maximum. More luminous SNe Ia have later, and brighter, secondary maxima. This is thought to be a result of the higher opacity in more luminous SNe Ia, which delays the onset of the recombination of Fe III to Fe II, the main driver of the secondary maximum.

No empirical corrections between luminosity and other light curve properties need to be applied to use SNe Ia as distance indicators in the NIR. Therefore, SNe Ia are often considered "standard" candles in the NIR, resulting in just a four percent uncertainty in the distance using $H$-band data (Barone-Nugent et al. 2012). Studies of SNe Ia as distance indicators in the NIR are more challenging than optical studies because of the increased difficulty in obtaining measurements at NIR compared to optical wavelengths. However, recent surveys have shown that due to their light curve homogeneity, only a single NIR light curve point (combined with a prior on the date of maximum light from optical light curves) is needed to produce a scatter of just six percent in the distance.

A key spectral feature around maximum light at NIR wavelengths is a C feature at 1.07 μm, which can be used to trace primordial, unprocessed white-dwarf material. A strong Mg feature is also visible in NIR spectra and can be used to probe the conditions under which a transition from deflagration to detonation occurs (Wheeler et al. 1998). After the secondary maximum has occurred, the NIR spectra of SNe Ia transition to being dominated by features from Fe-group elements. At epochs greater than $\sim$150 d, the NIR spectra of SNe Ia, as seen in the optical spectra, are dominated by forbidden emission lines of Fe-group elements, in particular [Fe II].

Mid-infrared (MIR) observations ($\sim$3.6–13 μm) of SNe Ia are limited, with MIR spectra existing for only three SNe Ia (Gerardy et al. 2007; Telesco et al. 2015). Similar to optical and NIR wavelengths at similar epochs, the spectra are dominated by Co, Fe, and Ni, but with the addition of Ar lines ([Ar II], [Ar III]) that are unique to the MIR.

MIR photometry has been obtained for a handful of SNe Ia with Spitzer and Gran Telescopio Canarias in bands ranging from 3.6 to 22 μm (e.g., Gerardy et al. 2007). The MIR shows a similar decline after maximum light to the optical and NIR light curves. However, unlike the NIR light curves, there is no evidence of a secondary maximum and the MIR light curves appear very homogenous. Constraints on the presence of preexisting dust can also be set using MIR observations.

## 2.5      Ultraviolet Properties

The percentage of flux released at UV wavelengths ($<4000\,\text{Å}$) is much lower than at optical wavelengths, with a maximum around peak of $\sim 10\,\%$ of the optical luminosity (Wang et al. 2009). SN Ia light curves in the UV follow a similar rise to peak and subsequent decline as seen in the optical. At early times, SN Ia UV flux is mainly formed through the process of "reverse fluorescence," where photons are scattered from longer to shorter wavelengths (Lucy 1999). The UV region is dominated by many overlapping metal lines, resulting in strong line blanketing. The UV photons that escape originate from the outermost ejecta, since UV photons produced deeper in the ejecta will be scattered to longer wavelengths before escaping. Therefore, UV wavelengths are sensitive to the metal abundance in the outer layers of the ejecta, which can be related back to the progenitor properties.

An increased dispersion in SN Ia light curves at UV compared to optical wavelengths is seen, likely caused by variations in the metal content (Ellis et al. 2008). UV photometry bands are typically not used in cosmology studies because of this increased scatter, as well as the observed evolution in SN Ia UV spectra with redshift (Foley et al. 2012; Maguire et al. 2012). The evolution is in the sense that SNe Ia at higher redshift have a stronger near-UV flux compared to those at low redshift.

UV spectra at nebular epochs have not been obtained. UV spectra at nebular epochs are predicted to contain little flux; multiple scatterings and the absorption of UV photons and remission at longer wavelengths (fluorescence) result in a transfer of the UV emissivity to longer wavelengths. Similarly to the optical and NIR, any features that do appear would be expected to be due to Fe-group elements.

## 2.6      Gamma-Ray Observations of Radioactive Decay

The detection of gamma rays produced by the decay chain of $^{56}$Ni in SNe Ia can provide important information on their explosion physics. However, observations are difficult to obtain for even the most nearby SNe Ia, with expected signals of just one percent of the background. Specialized gamma-ray observatories must be used, such as the European Space Agency's space-based observatory, INTEGRAL, which measures gamma rays in the range 15 keV to 10 MeV.

Using INTEGRAL, the early-time gamma-ray signal from the very nearby (3.3 Mpc), SN 2014J was investigated. Gamma rays from the initial decay of $^{56}$Ni at 158 and 812 keV were tentatively identified at $\sim 20$ d after explosion by Diehl et al. (2014), but not seen by Churazov et al. (2015). If real, this detection is much earlier than the predicted timescale of several weeks for gamma-ray emergence (Isern et al. 2008; Sim and Mazzali 2008), suggesting that radioactive material is present much farther out in the ejecta than predicted by nearly all explosion models.

At later times ($\sim 90$–100 d after explosion), gamma rays produced by the radioactive decay of $^{56}$Co should be able to escape the SN ejecta, as the envelope
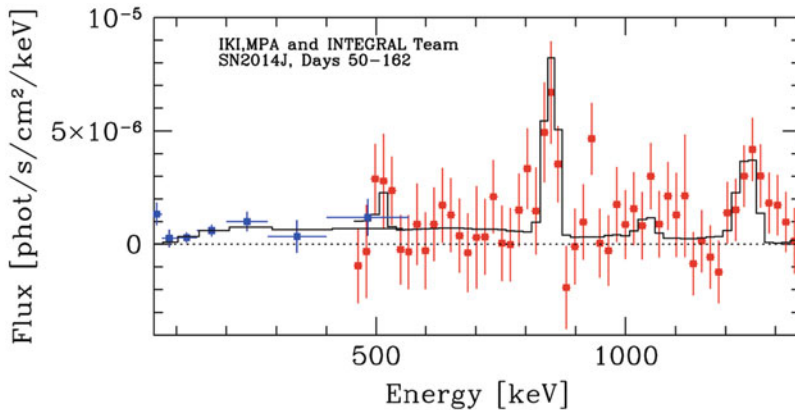
**Fig. 6** Gamma-ray spectrum of SN 2014J obtained with INTEGRAL in the range 50–162 d post explosion. Data in *blue* is from the ISGRI instrument on INTEGRAL, while data in *red* is from the SPI instrument. The *black solid line* is a model fit to the spectrum. Reproduced by permission of the AAS from Churazov et al. (2015). Flux excesses are seen at 847 and 1238 keV, consistent with lines of $^{56}$Co decay

expands and becomes more transparent to gamma rays. This was observed for the first time for SN 2014J at 847 and 1238 keV (see Fig. 6). Measurements of these line fluxes can give a direct estimate of the amount of radioactive $^{56}$Ni synthesized in the explosion. For SN 2014J, the measured fluxes corresponded to $\sim$0.5–0.6 M$_\odot$ of radioactive $^{56}$Ni, in excellent agreement with other estimates of the $^{56}$Ni mass produced.

## 2.7    Polarization Signatures of SNe Ia

Polarization measurements of SNe can provide information about the geometry of the ejecta, in particular the presence of asymmetries. The magnitude of polarization signatures in "normal" SNe Ia is, in general, small. Measurements of the continuum polarization probe the shape of the photosphere; for normal SNe Ia, the size of the continuum polarization is typically a few tenths of a percent, suggesting departures from spherical symmetry of <10 % (Hoeflich 1991; Wang et al. 1997). For subluminous SNe Ia, the continuum polarization levels are higher ($\sim$15 %), suggestive of an oblate ellipsoidal geometry of the ejecta.

Line polarization has been identified in a number of SN Ia spectral features. Significant polarization has been observed across the Si II and Ca II features at early times (e.g., Leonard et al. 2005; Patat et al. 2009; Wang et al. 2006). The high-velocity component of the Ca II NIR triplet can be highly polarized before maximum light and comes from line-forming regions orthogonal in the plane of the sky to the photospheric velocity component. This is possible to explain with a clumpy shell or torus of material (Kasen et al. 2003). These line polarization signals

are found to become weaker with time suggesting that it is the outer layers of the ejecta that are most asymmetric.

## 2.8    Host Galaxies and SN Ia Rates

Unlike core-collapse SNe that are exclusively associated with star-forming regions and young stellar populations, SNe Ia occur in a wide range of galaxy types,from dwarf irregulars to massive elliptical and spiral galaxies. The observed properties of SNe Ia are found to depend on the properties of their host galaxies, such as morphology, age, star-formation rate, mass, and metallicity (e.g., Hamuy et al. 1996, 2000; Sullivan et al. 2006). For example, more luminous SNe Ia occur preferentially in galaxies with younger stellar populations and more ongoing star formation, while fainter SNe Ia are more associated with older stellar populations and little ongoing star formation. This suggests that the properties of the stellar systems that produce SNe Ia are influenced by their environments, and this in turn impacts nonnegligibly on the observed properties of the SNe Ia themselves. The driving force behind these associations is currently unclear: are they caused by differences in the age of the systems at the time of explosion? Or perhaps the metal content of the SN explosion site?

The rate of SNe Ia exploding in different host environments is not constant, with SNe Ia being an order of magnitude more common in star-forming host galaxies (Mannucci et al. 2005; Sullivan et al. 2006). The "delay-time distribution," the rate of SNe Ia as a function of the time between star formation and a SN Ia explosion, is used to quantify the age distribution of the stellar populations producing SNe Ia. This in turn provides information on the underlying population of stellar systems that explode as SNe Ia. The tail of the "delay-time distribution" ($>10^8$ yr) is theoretically predicted to follow $t^{-1}$, where $t$ is the time between a burst of star formation and SN Ia explosion. This power law is in agreement with double-degenerate progenitor scenario predictions (Greggio 2005; Yungelson and Livio 1998). Binary population synthesis calculations suggest that SNe Ia occurring through a single-degenerate channel will explode between a few 100 million years and a few Gyr after formation (e.g., Claeys et al. 2014; Mennekens et al. 2010). Current data is well fit by a $t^{-1}$ power law at late times, but does not exclude a contribution to the SN Ia rate from single-degenerate channels at short delay times.

## 3    Progenitors

A stellar system that explodes as a SNe Ia has never been directly detected and it is not confirmed what types of stellar systems produce SNe Ia. Any information we have on their progenitor systems comes from indirect methods. Constraining the progenitor systems and explosion mechanisms of SNe Ia is currently a major area of SN research, with disagreement existing over the progenitor channel(s) that produce

the bulk of normal SNe Ia. In this section, a summary of the pros and cons for the main potential progenitor scenarios is described.

## 3.1    Single-Degenerate Models

In the single-degenerate scenario, the primary white dwarf accretes matter from a nondegenerate companion star until it approaches the Chandrasekhar mass limit and explodes (Nomoto 1982; Whelan and Iben 1973). The companion star can be a main sequence, He, subgiant, or giant star. Accretion is expected to occur via a stellar wind or through Roche-lobe overflow, where some of the donor-star material lies outside its Roche lobe and is no longer gravitationally bound.

A problem with many single-degenerate scenarios is that some fine-tuning is required for the white dwarf to not only accrete matter from the companion star but also to grow in mass (Nomoto 1982). Mass can be lost through nova eruptions, helium flashes, or disk winds. If the accretion rate is too low, the hydrogen-rich material is burnt at the same rate it is accreted, resulting in no mass growth. If the accretion rate is too high, the accreted material builds up in an expanded red giant-like configuration, which engulfs the donor star and halts further accretion. Therefore, theoretically there is only a narrow range of mass accretion rates where the white dwarf can accrete the companion star material in a stable configuration.

However, a number of observed recurrent novae exist that are plausible single-degenerate SN Ia progenitor systems (Darnley et al. 2015). These contain high-mass white dwarfs that are close to the Chandrasekhar mass and are successfully accreting mass at a high rate. There are ten confirmed recurrent nova systems in our Galaxy, but more classical novae may be recurrent novae but a second outburst has just not been observed. Pagnotta and Schaefer (2014) predicted that 9–38 % of the ∼400 known Galactic novae may be recurrent novae with recurrence times of <100 yr.

## 3.2    Double-Degenerate Models

In the double-degenerate scenario (Iben and Tutukov 1984; Webbink 1984), the explosion of the primary carbon-oxygen white dwarf occurs in a binary containing another white dwarf. There are many theoretical predictions of what exactly triggers the primary white dwarf to explode: the steady accretion of the secondary white dwarf onto the primary which reaches the Chandrasekhar mass and explodes, the violent merger of the two white dwarfs which triggers a carbon detonation, or the so-called "double-detonation" scenario, where the detonation of He on the primary white-dwarf surface triggers a carbon detonation in its core that unbinds the star.

### 3.2.1    Dynamical Mergers

The classical Chandrasekhar mass double-degenerate model involves the tidal disruption and accretion of the less massive white dwarf onto the primary white dwarf. This accretion takes place on a dynamical timescale ($\sim 10^5$ yr) with the

primary white dwarf eventually approaching the Chandrasekhar mass, triggering carbon burning, and a runaway thermonuclear explosion. The main difficulty with this scenario is that when carbon and oxygen from the secondary star are accreted too fast, then carbon is ignited off-center in the primary white dwarf producing a neon-oxygen-magnesium white dwarf. Electron capture on the neon and magnesium then induces collapse to a neutron star, ("accretion-induced collapse") instead of a thermonuclear explosion (Nomoto and Iben 1985). However, if the accretion rate is low enough ($<10^{-5}\,M_\odot\,yr^{-1}$) and the temperature is below that required to ignite carbon, then a Chandrasekhar mass explosion may still be possible.

### 3.2.2   Violent Mergers

The merger of two white dwarfs can produce a so-called violent merger (Pakmor et al. 2010). Gravitational wave emission from the binary system leads to a shrinking of its orbit to the point where the white dwarfs are close enough to interact. The less massive white dwarf is accreted onto the primary initially stably but then violently, where the primary becomes compressed and its surface is heated. The crucial issue for producing a detonation is determining whether hotspots that would lead to carbon detonation are produced on the surface. There is some disagreement in the models about if and how hotspots form. A way around the uncertainty in their formation is to invoke a thin layer of He ($\sim$0.01 $M_\odot$) on the surface of the white dwarf. This He layer ignites in the violent merger and triggers a converging shock wave that causes a secondary detonation of the core. This mechanism is similar to the "double-detonation" scenario.

### 3.2.3   Double Detonations

Double detonations are a recently revived theory that could potentially solve many of the problems associated with other SN Ia progenitor models. However, the rate of these systems is uncertain. The explosion mechanism involves a layer of He on the surface of the primary white dwarf which ignites, resulting in a second detonation of the carbon in the core of the star. The original models of double detonations were of accretion of He from a nondegenerate He star companion, with an accreted He layer of $\sim$0.2 $M_\odot$ of material (Nomoto 1982; Nomoto and Sugimoto 1977; Woosley et al. 1986). These masses of He were generally too large not to leave strong observable signatures in the SN Ia spectra, such as He-burning products like carbon and oxygen, that are not seen. However, He masses that are 10–100 times smaller now appear capable of triggering a He-shell detonation and hence a secondary core detonation, without appreciable He signatures being visible in the SN spectra (Bildsten et al. 2007; Shen and Bildsten 2014).

### 3.2.4   Other Scenarios

Other progenitor scenarios have been put forward to explain SNe Ia, but are still somewhat in their infancy in terms of testing and modeling efforts. One alternative method to explode a carbon-oxygen white dwarf is in a head-on collision with another white dwarf. This collision could be induced by a dense stellar environment such as that found in globular clusters or by a third low-mass body orbiting around

the inner binary white-dwarf system ("hierarchical triple system"). This third body causes the eccentricity of this inner white-dwarf binary to increase via Kozai oscillations (Kozai 1962) and could result in a head-on collision in some cases. However, the rate of triple systems with inner white-dwarf binaries is expected to be low – at most 10–20 % of stars are in triple systems, with much lower numbers containing two inner white dwarfs.

The merger of a white dwarf and the core of an asymptotic giant branch star near the end of the common envelope phase has also been hypothesized to result in a SN Ia (Kashi and Soker 2011). The rate of these systems is not well constrained but they may be responsible for some unusual SNe Ia with large quantities of circumstellar material such as PTF11kx (Soker et al. 2013).

## 3.3 Observing Progenitor Signatures

Given the controversy over what progenitor channel (or channels) produce SNe Ia, much SN Ia research has focused on trying to disentangle subtle signatures of how they exploded from the broad SN signatures. In this section, we discuss a number of methods for constraining the progenitor systems of SNe Ia.

### 3.3.1 Interaction with Companion Stars

Early-time light curves have been studied to look for interaction with companion stars in the single-degenerate scenario. The initial interaction between the SN ejecta and a companion star produces an X-ray flash on the timescale of minutes (Kasen 2010). UV and optical emission from the interaction may be visible from 1–5 d after explosion. A tentative detection was made for SN 2012cg (Marion et al. 2016), while no interaction was seen in high-cadence Kepler observations of three SNe Ia (Olling et al. 2015).

Low-velocity ($<1000\,\mathrm{km\,s^{-1}}$) H- and He-rich material is expected to result from the stripping or ablating of material from a nondegenerate companion star due to impact of the SN Ia ejecta (Liu et al. 2012; Pan et al. 2012; Wheeler et al. 1975). Due to its low velocities, it is only visible when the outer high-velocity layers have become optically thin at $>200$ d after explosion. The amount of unbound material depends on the nature of the companion star: red giants ($0.6\,M_\odot$), main sequence stars ($0.1$–$0.2\,M_\odot$), and He stars ($0.02$–$0.06\,M_\odot$). Observational studies of nearby SNe Ia have not conclusively detected H or He-rich material (e.g., Leonard 2007). Using the spectral modeling analysis of Mattila et al. (2005), limits of $<0.001$–$0.06\,M_\odot$ on the amount of unbound H-rich material have been placed, with the most constraining limits for SN 2011fe and SN 2014J.

### 3.3.2 Circumstellar Material

The presence of circumstellar material was originally thought to be a key discriminant of SN Ia progenitor channels. This non-accreted companion star material was expected to be present only when the companion star to the white dwarf was a nondegenerate star. However, new modeling of double-degenerate systems has

suggested that these channels may also produce circumstellar material during the common envelope phase or through the interaction of material ejected from the binary system with the interstellar medium (Raskin and Kasen 2013; Shen et al. 2013).

The first detection of circumstellar material in a SN Ia system was made for SN 2006X using high-resolution spectroscopy (Patat et al. 2007). This was detected through the presence of blueshifted Na I D absorption features in the SN spectra. Narrow absorption features of Na I D are often seen in astronomical spectra. They normally arise from interstellar absorption both in the Milky Way and in external galaxies. Crucially in spectra of SN 2006X, the strength of the Na I D features was time varying suggesting an origin in the circumstellar material of the progenitor system. These time-varying features have now been observed in a number of SNe Ia. Larger statistical samples of Na I D features in SN Ia spectra have found that ~20 % of SNe Ia are displaying signatures of outflowing material consistent with circumstellar material, and there may be a connection between their presence and the SN properties (Sternberg et al. 2011).

### 3.3.3 Radio/X-Ray Studies of the Circumbinary Environment

Radio and X-ray signals from SNe Ia are created by the interaction of the SN blast wave with circumstellar material present in the SN environment. Therefore, radio and X-ray observations are excellent probes of the environment into which the SN explodes. However, no detection of radio or X-ray emission from a SN Ia within 1 year of explosion has been made.

Radio synchrotron is produced when the interaction between the blast wave of the SN and the circumstellar medium accelerates electrons to relativistic speeds generating strong magnetic fields. These relativistic electrons also up-scatter optical photons, producing emission via inverse Compton scattering at X-ray wavelengths.

Radio non-detection limits of 95 SNe Ia (including some unusual sub-classes) from the Very Large Array were analyzed (Chomiuk et al. 2016). From these non-detections, limits on the mass-loss rate of the system prior to the explosion in the range of $10^{-9}$–$10^{-4}$ $M_\odot$ yr$^{-1}$ were determined, ruling out red giant companions for >90 % of SNe Ia. Non-detections of X-ray emission for two nearby SNe Ia, SNe 2011fe and 2014J, place similar mass-loss limits ($10^{-9}$ $M_\odot$ yr$^{-1}$), again ruling out symbiotic systems and those with steady mass loss prior to explosion (Horesh et al. 2012; Margutti et al. 2014).

### 3.3.4 Pre-explosion Progenitor Searches

Unlike core-collapse SNe, the progenitor system of a normal SN Ia has never been directly detected in pre-explosion imaging. This is because the progenitor systems of SNe Ia are intrinsically much fainter than the massive star systems that produce core-collapse SNe. The best non-detection limit on the progenitor system from pre-explosion imaging is for SN 2011fe (Li et al. 2011). For this very nearby SN Ia, a system containing a luminous giant companion or most helium stars can be ruled out (Fig. 7). This suggests the companion star was either another white dwarf or had a main sequence, faint red giant, or subgiant companion.
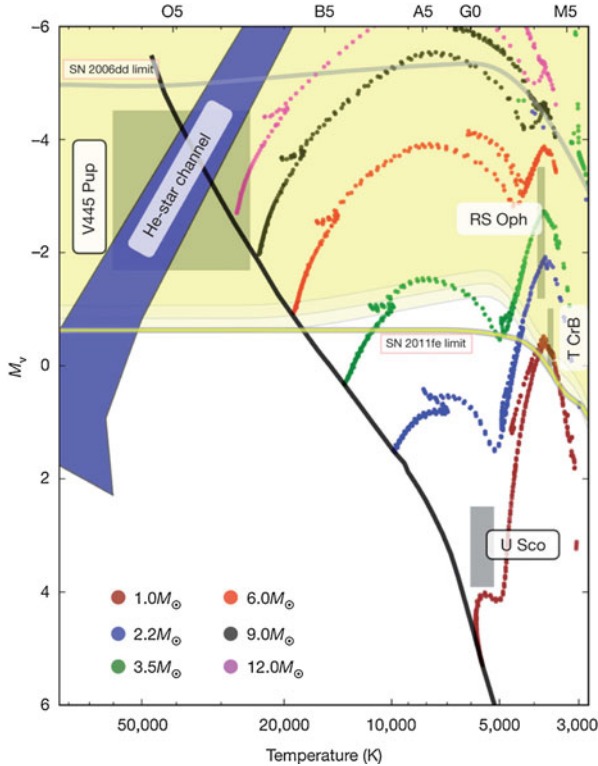
**Fig. 7** Hertzsprung-Russell diagram (absolute *V*-band magnitude against effective temperature) showing the $2\sigma$ limit (*thick yellow line*) for the progenitor system of SN 2011fe set by Hubble Space Telescope pre-explosion imaging from Li et al. (2011). Theoretical evolutionary tracks of isolated solar-metallicity stars with masses in the range $1-12\,M_\odot$ are shown, along with theoretical estimates for He-star channels and observed candidate systems. The observational limit from Hubble Space Telescope imaging of another nearby SN Ia, SN 2006dd, is shown for comparison. The Hubble Space Telescope pre-explosion imaging for SN 2011fe rules out luminous red giants and almost all helium stars as the companions star to the primary white dwarf (Reprinted by the permission from Macmillan Publishers Ltd: Nature from publication Li et al. 2011)

## 4 Conclusions

While the continued use of SNe Ia as cosmological probes is certain, observations have yet to unravel the mystery of their progenitor systems and explosion mechanisms. SNe Ia are incredibly energetic events that result from the thermonuclear explosion of white dwarfs through interaction with a companion star and produce $\sim 0.7\,M_\odot$ of $^{56}$Ni each. They are mainly an optical phenomenon, but dedicated observations from gamma rays to radio have uncovered a wealth of information outside the optical regime. Although to first-order SNe Ia are a homogenous class of objects, there is a surprising diversity observed in their light curves, spectra,

and host-galaxy environments. Some of this diversity has now been explained with detailed theoretical modeling, but there is still much to be learnt. Although a very nearby SN Ia (in particular a Galactic event) would be incredibly useful for testing theories, individual objects have obvious limitations – even if the progenitor system was unveiled for one SN Ia, this would tell us relatively little about the class of SNe Ia as a whole. Therefore, while the use of SNe Ia as cosmological distance indicators mainly drives the need for further high-precision samples, larger, better-understood samples are also needed to improve our understanding of the underlying physical processes that create these cosmic lighthouses.

## 5   Cross-References

► Dynamical Mergers
► Evolution of Accreting White Dwarfs to the Thermonuclear Runaway
► Explosion Physics of Thermonuclear Supernovae and Their Signatures
► Introduction to Supernova Polarimetry
► Light Curves of Type I Supernovae
► Nucleosynthesis in Thermonuclear Supernovae
► Observational and Physical Classification of Supernovae
► Spectra of Supernovae During the Photospheric Phase
► Spectra of Supernovae in the Nebular Phase
► Supernova Cosmology in the Big Data Era
► The Extremes of Thermonuclear Supernovae
► The Infrared Hubble Diagram of Type Ia Supernovae
► The Peak Luminosity-Decline Rate Relationship for Type Ia Supernovae
► Thermonuclear Explosions of Chandrasekhar Mass White Dwarfs
► Type Ia supernovae
► Violent Mergers

## References

Arnett WD (1982) Type I supernovae. I – Analytic solutions for the early part of the light curve. ApJ 253:785
Axelrod TS (1980) PhD thesis, California Univ., Santa Cruz
Barone-Nugent RL et al (2012) Near-infrared observations of Type Ia supernovae: the best known standard candle for cosmology. MNRAS 425:1007
Betoule M et al (2014) Improved cosmological constraints from a joint analysis of the SDSS-II and SNLS supernova samples. A&A 568:A22
Bildsten L, Shen KJ, Weinberg NN, Nelemans G (2007) Faint thermonuclear supernovae from AM canum venaticorum binaries. ApJ 662:L95
Bloom JS et al (2012) A compact degenerate primary-star progenitor of SN 2011fe. ApJ 744:L17
Chomiuk L et al (2016) A deep search for prompt radio emission from thermonuclear supernovae with the very large array. ApJ 821:119
Churazov E et al (2015) Gamma-rays from Type Ia supernova SN 2014J. ApJ 812:62

Claeys JSW, Pols OR, Izzard RG, Vink J, Verbunt FWM (2014) Theoretical uncertainties of the Type Ia supernova rate. A&A 563:A83

Colgate SA, McKee C (1969) Early supernova luminosity. ApJ 157:623

Conley A et al (2008) SiFTO: An empirical method for fitting SN Ia light curves. ApJ 681:482

Darnley MJ et al (2015) A remarkable recurrent nova in M31: discovery and optical/UV observations of the predicted 2014 eruption. A&A 580:A45

Diehl R et al (2014) Early $^{56}$Ni decay gamma rays from SN 2014J suggest an unusual explosion. Science 345:1162

Ellis RS et al (2008) Verifying the cosmological utility of Type Ia supernovae: implications of a dispersion in the ultraviolet spectra. ApJ 674:51

Filippenko AV (1997) Optical spectra of supernovae. ARA&A 35:309

Firth RE et al (2015) The rising light curves of Type Ia supernovae. MNRAS 446:3895

Foley RJ et al (2012) A Mismatch in the ultraviolet spectra between low-redshift and intermediate-redshift Type Ia supernovae as a possible systematic uncertainty for supernova cosmology. AJ 143:113

Fransson C, Jerkstrand A (2015) Reconciling the infrared catastrophe and observations of SN 2011fe ApJ 814:L2

Ganeshalingam M et al (2010) Results of the lick observatory supernova search follow-up photometry program: BVRI light curves of 165 type Ia supernovae. ApJS 190:418

Gerardy CL et al (2004) SN 2003du: signatures of the circumstellar environment in a normal Type Ia supernova? ApJ 607:391

Gerardy CL et al (2007) Signatures of delayed detonation, asymmetry, and electron capture in the mid-infrared spectra of supernovae 2003hv and 2005df. ApJ 661:995

Greggio L (2005) The rates of type Ia supernovae. I. Analytical formulations. A&A 441:1055

Guy J, Astier P, Nobili S, Regnault N, Pain R (2005) SALT: a spectral adaptive light curve template for type Ia supernovae. A&A 443:781

Hamuy M, Phillips MM, Suntzeff NB, Schommer RA, Maza J, Aviles R (1996) The absolute luminosities of the Calan/Tololo Type IA supernovae. AJ 112:2391

Hamuy M et al (2000) A search for environmental effects on Type IA supernovae. AJ 120:1479

Hicken M et al (2009) CfA3: 185 Type Ia supernova light curves from the CfA. ApJ 700:331

Hoeflich P, Khokhlov A, Wheeler JC, Phillips MM, Suntzeff NB, Hamuy M (1996) Maximum brightness and postmaximum decline of light curves of Type IA supernovae: a comparison of theory and observations. ApJ 472:L81+

Hoeflich P (1991) Asphericity effects in scattering dominated photospheres. A&A 246:481

Horesh A et al (2012) Early radio and X-ray observations of the youngest nearby Type Ia supernova PTF 11kly (SN 2011fe). ApJ 746:21

Iben I, Tutukov AV (1984) Supernovae of type I as end products of the evolution of binaries with components of moderate initial mass (M not greater than about 9 solar masses). ApJS 54:335

Isern J, Bravo E, Hirschmann A (2008) Detection and interpretation of $\gamma$-ray emission from SN Ia. New A 52:377

Jha S, Riess AG, Kirshner RP (2007) Improved distances to Type Ia supernovae with multicolor light-curve shapes: MLCS2k2. ApJ 659:122

Kasen D (2010) Seeing the collision of a supernova with its companion star. ApJ 708:1025

Kasen D et al (2003) Analysis of the flux and polarization spectra of the Type Ia supernova SN 2001el: exploring the geometry of the high-velocity ejecta. ApJ 593:788

Kasen D, Woosley SE (2007) On the origin of the Type Ia supernova width-luminosity relation. ApJ 656:661

Kashi A, Soker N (2011) A circumbinary disc in the final stages of common envelope and the core-degenerate scenario for Type Ia supernovae. MNRAS 417:1466

Kozai Y (1962) Secular perturbations of asteroids with high inclination and eccentricity. AJ 67:591

Krisciunas K et al (2004) Optical and infrared photometry of the Type Ia supernovae 1991T, 1991bg, 1999ek, 2001bt, 2001cn, 2001cz, and 2002bo. AJ 128:3034

Leonard DC (2007) Constraining the Type Ia supernova progenitor: the search for hydrogen in nebular spectra. ApJ 670:1275

Leonard DC, Li W, Filippenko AV, Foley RJ, Chornock R (2005) Evidence for spectropolarimetric diversity in Type Ia supernovae. ApJ 632:450

Li W et al (2011) Exclusion of a luminous red giant as a companion star to the progenitor of supernova SN 2011fe. Nature 480:348

Liu ZW et al (2012) Three-dimensional simulations of the interaction between Type Ia supernova ejecta and their main sequence companions. A&A 548:A2

Lucy LB (1999) Improved Monte Carlo techniques for the spectral synthesis of supernovae. A&A 345:211

Maeda K et al (2010) An asymmetric explosion as the origin of spectral evolution diversity in type Ia supernovae. Nature 466:82

Maguire K et al (2012) Hubble space telescope studies of low-redshift Type Ia supernovae: evolution with redshift and ultraviolet spectral trends. MNRAS 426:2359

Maguire K et al (2014) Exploring the spectral diversity of low-redshift Type Ia supernovae using the palomar transient factory. MNRAS 444:3258

Mannucci F et al (2005) The supernova rate per unit mass. A&A 433:807

Margutti R et al(2014) No X-rays from the very nearby Type Ia SN 2014J: constraints on its environment. ApJ 790:52

Marion GH et al (2016) SN~2012cg: evidence for interaction between a normal Type Ia supernova and a non-degenerate binary companion. ApJ 820:92

Mattila S et al (2005) Early and late time VLT spectroscopy of SN 2001el – progenitor constraints for a type Ia supernova. A&A 443:649

Mazzali PA et al (2005) High-velocity features: a ubiquitous property of Type Ia supernovae. ApJ 623:L37

Mazzali PA et al (2015) Nebular spectra and abundance tomography of the Type Ia supernova SN 2011fe: a normal SN Ia with a stable Fe core. MNRAS 450:2631

Mazzali PA et al (2014) Hubble space telescope spectra of the Type Ia supernova SN 2011fe: a tail of low-density, high-velocity material with $Z > Z_{solar}$. MNRAS 439:1959

Mennekens N, Vanbeveren D, De Greve JP, De Donder E (2010) The delay-time distribution of Type Ia supernovae: a comparison between theory and observation. A&A 515:A89

Nomoto K (1982) Accreting white dwarf models for type I supernovae. I – Presupernova evolution and triggering mechanisms. ApJ 253:798

Nomoto K, Iben I (1985) Carbon ignition in a rapidly accreting degenerate dwarf – A clue to the nature of the merging process in close binaries. ApJ 297:531

Nomoto K, Sugimoto D (1977) Rejuvenation of helium white dwarfs by mass accretion. PASJ 29:765

Nugent P, Phillips M, Baron E, Branch D, Hauschildt P (1995) Evidence for a spectroscopic sequence among Type 1a supernovae. ApJ 455:L147+

Nugent PE et al (2011) Supernova SN 2011fe from an exploding carbon-oxygen white dwarf star. Nature 480:344

Olling RP et al (2015) No signature of ejecta interaction with a stellar companion in three type Ia supernovae. Nature 521:332

Pagnotta A, Schaefer BE (2014) Identifying and quantifying recurrent Novae masquerading as classical novae. ApJ 788:164

Pakmor R, Kromer M, Röpke FK, Sim SA, Ruiter AJ, Hillebrandt W (2010) Sub-luminous type Ia supernovae from the mergers of equal-mass white dwarfs with mass ~0.9M$_{solar}$. Nature 463:61

Pan K-C, Ricker PM, Taam RE (2012) Impact of Type Ia supernova ejecta on binary companions in the single-degenerate scenario. ApJ 750:151

Patat F, Baade D, Höflich P, Maund JR, Wang L, Wheeler JC (2009) VLT spectropolarimetry of the fast expanding type Ia SN 2006X. A&A 508:229

Patat F et al (2007) Detection of circumstellar material in a normal Type Ia supernova. Science 317:924

Perlmutter S et al (1999) Measurements of omega and lambda from 42 high-redshift supernovae. ApJ 517:565

Philipp M. M. (1993) The absolute magnitudes of Type IA supernovae. ApJ, 413, 105L

Piro AL, Nakar E (2014) Constraints on shallow $^{56}$Ni from the early light curves of Type Ia supernovae. ApJ 784:85

Raskin C, Kasen D (2013) Tidal tail ejection as a signature of Type Ia supernovae from white dwarf mergers. ApJ 772:1

Riess AG et al (1998) Observational evidence from supernovae for an accelerating Universe and a cosmological constant. AJ 116:1009

Riess AG, Press WH, Kirshner RP (1996) A precise distance indicator: Type IA supernova multicolor light-curve shapes. ApJ 473:88

Shen KJ, Bildsten L (2014) The ignition of carbon detonations via converging shock waves in white dwarfs. ApJ 785:61

Shen KJ, Guillochon J, Foley RJ (2013) Circumstellar absorption in double detonation Type Ia supernovae. ApJ 770:L35

Sim SA, Mazzali PA (2008) On the $\gamma$-ray emission of Type Ia supernovae. MNRAS 385:1681

Soker N, Kashi A, García-Berro E, Torres S, Camacho J (2013) Explaining the Type Ia supernova PTF 11kx with a violent prompt merger scenario. MNRAS 431:1541

Sollerman J et al (2004) The late-time light curve of the type Ia supernova 2000cx. A&A 428:555

Sternberg A et al (2011) Circumstellar material in Type Ia supernovae via sodium absorption features. Science 333:856

Stritzinger MD et al (2011) The carnegie supernova project: second photometry data release of low-redshift Type Ia supernovae. AJ 142:156

Sullivan M et al (2006) Rates and properties of Type Ia supernovae as a function of mass and star formation in their host galaxies. ApJ 648:868

Telesco CM et al (2015) Mid-IR Spectra of Type Ia SN 2014J in M82 Spanning the First 4 Months. ApJ 798:93

Thomas RC et al (2011) Type Ia supernova carbon footprints. ApJ 743:27

Tripp R. (1998) A two-parameter luminosity correction for Type IA supernovae. A&A, 331, 815

Wang L et al (2006) Premaximum spectropolarimetry of the Type Ia SN 2004dt. ApJ 653:490

Wang L, Höflich P, Wheeler JC (1997) Supernovae and their host galaxies. ApJ 483:L29

Wang X et al (2009) The golden standard Type Ia supernova 2005cf: observations from the ultraviolet to the near-infrared wavebands. ApJ 697:380

Webbink RF (1984) Double white dwarfs as progenitors of R Coronae Borealis stars and Type I supernovae. ApJ 277:355

Wheeler JC, Höflich P, Harkness RP, Spyromilio J (1998) Explosion diagnostics of Type IA supernovae from early infrared spectra. ApJ 496:908

Wheeler JC, Lecar M, McKee CF (1975) Supernovae in binary systems. ApJ 200:145

Whelan J, Iben IJ (1973) Binaries and supernovae of Type I. ApJ 186:1007

Woosley SE, Taam RE, Weaver TA (1986) Models for Type I supernova. I – detonations in white dwarfs. ApJ 301:601

Yungelson L, Livio M (1998) Type IA supernovae: an examination of potential progenitors and the redshift distribution. ApJ 497:168